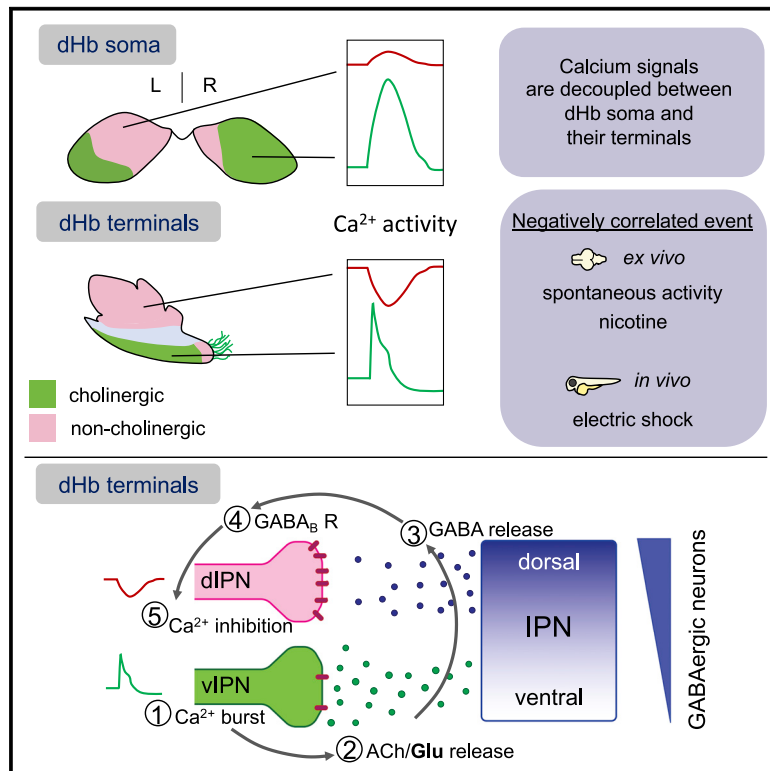


# Current Biology

## Trans-inhibition of axon terminals underlies competition in the habenulo-interpeduncular pathway

### Graphical abstract



### Authors

Margherita Zaupa,  
Seyedeh Maryam Alavi Naini,  
Maroun Abi Younes, ...,  
Marnie E. Halpern, Jean-Marie Mangin,  
Elim Hong

### Correspondence

elim.hong@inserm.fr

### In brief

Zaupa et al. show that calcium signals in habenular soma are not reflective of activity in axon terminals at the interpeduncular nucleus. They uncover an atypical mode of lateral inhibition between two habenular circuits where the activation of cholinergic neurons inhibits non-cholinergic activity by retrograde signaling from their target site.

### Highlights

- Calcium signals in habenular (Hb) soma do not reflect axon terminal activity
- Synchronized Hb cholinergic activity inhibits non-cholinergic terminals
- Presynaptic inhibition of non-cholinergic terminals is mediated by GABA<sub>B</sub> receptors
- GABA<sub>B</sub> R activation by retrograde signaling from the interpeduncular nucleus

Article

# Trans-inhibition of axon terminals underlies competition in the habenulo-interpeduncular pathway

Margherita Zauza,<sup>1,6</sup> Seyedeh Maryam Alavi Naini,<sup>1,6</sup> Maroun Abi Younes,<sup>1</sup> Erika Bullier,<sup>1</sup> Erik R. Duboué,<sup>2</sup> Hervé Le Corronc,<sup>1</sup> Hédi Soula,<sup>3</sup> Sebastian Wolf,<sup>4</sup> Raphaël Candelier,<sup>4</sup> Pascal Legendre,<sup>1</sup> Marnie E. Halpern,<sup>5</sup> Jean-Marie Mangin,<sup>1</sup> and Elim Hong<sup>1,7,\*</sup>

<sup>1</sup>INSERM, CNRS, Neurosciences Paris Seine - Institut de Biologie Paris Seine (NPS - IBPS), Sorbonne Université, 75005 Paris, France

<sup>2</sup>Jupiter Life Science Initiative, Wilkes Honors College and Charles E. Schmidt College of Science, Florida Atlantic University, Jupiter, FL 33458, USA

<sup>3</sup>INSERM, Sorbonne Université, Nutriomics, La Pitié Salpêtrière, 75013 Paris, France

<sup>4</sup>Laboratoire Jean Perrin, CNRS, Sorbonne Université, 75005 Paris, France

<sup>5</sup>Department of Molecular and Systems Biology, Geisel School of Medicine at Dartmouth, Hanover, NH 03755, USA

<sup>6</sup>These authors contributed equally

<sup>7</sup>Lead contact

\*Correspondence: [elim.hong@inserm.fr](mailto:elim.hong@inserm.fr)

<https://doi.org/10.1016/j.cub.2021.08.051>

## SUMMARY

Survival of animals is dependent on the correct selection of an appropriate behavioral response to competing external stimuli. Theoretical models have been proposed and underlying mechanisms are emerging to explain how one circuit is selected among competing neural circuits. The evolutionarily conserved forebrain to midbrain habenulo-interpeduncular nucleus (Hb-IPN) pathway consists of cholinergic and non-cholinergic neurons, which mediate different aversive behaviors. Simultaneous calcium imaging of neuronal cell bodies and of the population dynamics of their axon terminals reveals that signals in the cell bodies are not reflective of terminal activity. We find that axon terminals of cholinergic and non-cholinergic habenular neurons exhibit stereotypic patterns of spontaneous activity that are negatively correlated and localize to discrete subregions of the target IPN. Patch-clamp recordings show that calcium bursts in cholinergic terminals at the ventral IPN trigger excitatory currents in IPN neurons, which precede inhibition of non-cholinergic terminals at the adjacent dorsal IPN. Inhibition is mediated through presynaptic GABA<sub>B</sub> receptors activated in non-cholinergic habenular neurons upon GABA release from the target IPN. Together, the results reveal a hard-wired mode of competition at the terminals of two excitatory neuronal populations, providing a physiological framework to explore the relationship between different aversive responses.

## INTRODUCTION

The bilaterally paired habenular nuclei (Hb) are part of the highly conserved dorsal diencephalic conduction system connecting the limbic forebrain with monoaminergic brainstem areas.<sup>1,2</sup> Anatomically, they consist of medial (MHb) and lateral (LHb) nuclei in mammals that are homologous to the dorsal (dHb) and ventral (vHb) nuclei of teleosts. The LHb and vHb send projections through the fasciculus retroflexus (FR) directly to serotonergic raphe neurons and dopaminergic neurons in the ventral tegmental area. Axons from MHb and dHb neurons course through the FR and terminate at an unpaired midbrain target, the interpeduncular nucleus (IPN). The Hb-IPN pathway is critical for understanding addiction and mood disorders due to its involvement in regulating behaviors, such as stress, anxiety, and fear learning.<sup>1,3–6</sup>

The MHb/dHb glutamatergic neurons are divided into those that co-release acetylcholine (cholinergic) or neuropeptides, including substance P (non-cholinergic) or somatostatin.<sup>7–9</sup> In

rodents, cholinergic and non-cholinergic neuronal populations project to central and peripheral IPN domains, respectively.<sup>7</sup> Gene expression analyses, fluorescent dye tracing, and transgenic reporters have demonstrated left-right differences between the bilateral dHb of larval zebrafish.<sup>5,10,11</sup> For example, cholinergic neurons are located mainly in the right dHb and project to the ventral IPN (vIPN), whereas non-cholinergic neurons are more abundant in the left dHb and innervate the dorsal IPN (dIPN) (Figure 1A).<sup>9,12</sup> In rodents, cholinergic and non-cholinergic MHb neurons receive afferent input from neurons located in the triangular septum (TS) and the bed of the anterior commissure (BAC), respectively.<sup>13</sup> Toxin-induced ablation of TS-cholinergic or BAC-non-cholinergic MHb projections selectively impaired anxiety or fear learning behaviors.<sup>3</sup> Conditional genetic deletion of cerebellin (Cbln) genes in the MHb, Cbln4 in cholinergic, or Cbln2 in non-cholinergic neurons affects freezing behavior or spatial learning, respectively.<sup>4</sup>

The dHb responds differently to external factors, such as light, odor, and aversive stimuli in zebrafish larvae.<sup>5,14,15</sup> Inhibition of

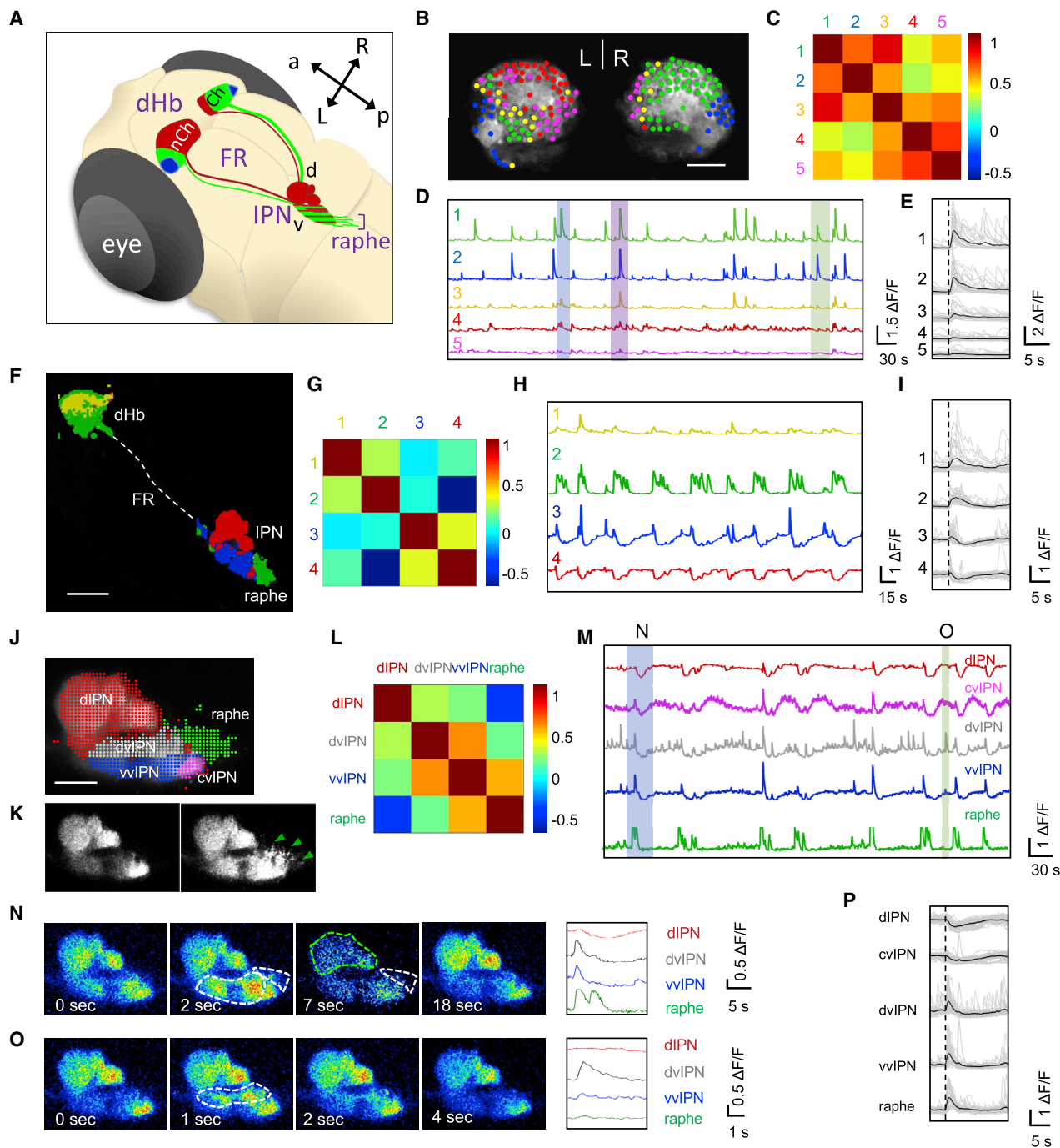


**Figure 1. Identification of functional domains in dHb-IPN pathway during spontaneous activity**

(A) Schematic of dHb-IPN pathway of larval zebrafish. Non-cholinergic (nCh) (red) neurons are mainly in the left dHb and project to the dorsal IPN (d), whereas cholinergic (Ch) (green) neurons are largely in the right dHb and project to the ventral IPN (v) and raphe (bracket). Somatostatinergic neurons are depicted in blue. Anterior (a), posterior (p), left (L), and right (R) are shown.

(B, F, and J) Representative 6 days post-fertilization (dpf) *Tg(gng8:GAL4<sup>ff</sup><sup>c426</sup>;Tg(UAS:GCaMP7a)* brain explants expressing GCaMP in dHb neurons (B), left dHb and their terminals (F), and terminals at the IPN and raphe (J), overlaid by colored circles representing functional domains identified by *k*-means clustering. Dotted line depicts the fasciculus retroflexus (FR) in (F).

(C, G, and L) Correlation matrix of average  $\Delta F/F$  signals between different clusters of dHb soma (C), dHb soma and terminals (G), and terminals at the IPN and raphe (L).

(D, H, and M) Average  $\Delta F/F$  traces from each cluster in 10-min recordings. Colored boxed events in (D) correspond to single-frame images in Figure S1.

(legend continued on next page)

neural transmission in the non-cholinergic (dHbL) versus cholinergic (dHbM) pathways in adult zebrafish is associated with winner or loser states in a social conflict paradigm.<sup>16</sup> Studies in rodents and zebrafish suggest that the cholinergic and non-cholinergic MHb/dHb neuronal populations form functionally distinct, parallel circuits. However, it is unknown whether the two pathways interact or directly influence the activity of one another.

To understand functional connectivity of the dHb-IPN pathway, we took advantage of the small size of the larval zebrafish brain to monitor neural activity in whole explant preparations. Calcium imaging revealed that dHb terminals at the IPN can be resolved into distinct domains based on their signaling dynamics. We discovered an inverse relationship between cholinergic and non-cholinergic neurons only at their axon terminals. Results from pharmacology, imaging, and electrophysiology experiments show that synchronized activity of cholinergic dHb neurons results in GABA release from the IPN, leading to presynaptic inhibition of non-cholinergic axon terminals. We propose a hardwired mode of competition between two neuronal populations, whereby synchronized activation of one group inhibits the activity of the other.

## RESULTS

### Cholinergic and non-cholinergic dHb terminals exhibit negatively correlated calcium events

The bilateral dHb on the dorsal surface of the diencephalon form connections with the IPN deeply embedded in the ventral midbrain, making it challenging to simultaneously monitor and manipulate both pre- and postsynaptic neuronal populations. To identify the hardwired mode of action of the dHb-IPN pathway, we analyzed spontaneous activity in both regions using brain explants from larval zebrafish. The entire brain was removed from *TgBAC(gng8:GAL4ff)<sup>c426</sup>;Tg(UAS:GCaMP7a)* larvae expressing GCaMP in dHb neuronal cell bodies and their terminals at the IPN.<sup>6</sup> We found that, whereas most dHb neurons exhibit spontaneous activity (Video S1; Figure S1A), a large cluster of neurons on the right together with a small cluster on the left exhibited correlated calcium bursts (Figures 1B–1E; Video S1). The neuronal clusters with highly correlated calcium bursts were consistently identified by *k*-means and hierarchical clustering methods (Figures 1B–1E and S1). Their location (Figures 1B and S1, green and blue) corresponds to that previously described for cholinergic and somatostatinergic neuronal clusters in the dHb (Figure 1A).<sup>9,12</sup>

We examined whether similar calcium signals were present in dHb axon terminals at the IPN. As the left dHb contains cholinergic and non-cholinergic neurons, which form connections with the

dorsal and ventral IPN (Figure 1A),<sup>9,12</sup> we carried out simultaneous calcium imaging of neurons in the left dHb and axon terminals at the IPN (Video S2). We used *k*-means clustering to identify domains in an unbiased manner because results were comparable with hierarchical clustering. Distinct domains of spontaneous activity defined stereotypic and correlated patterns of dHb neurons. The soma of the left dHb segregated into two (dorsal and ventral), and dHb axon terminals fell into three domains at the dorsal IPN (dIPN), ventral IPN (vIPN), and raphe nucleus (raphe) (Figure 1F). The activation pattern of ventral dHb soma clustered together with that of the raphe area, suggesting that these regions are functionally connected (Figure 1F, green). Surprisingly, we found that calcium signals in the dIPN were negatively correlated with those in the ventral dHb soma and raphe (Figures 1F–1I, red). When an increased calcium signal (burst) occurred in the soma of the ventral dHb and terminals at the raphe, a transient decrease from baseline calcium signaling (inhibition) was observed at the dIPN (Figures 1H and 1I). Calcium inhibition was limited to terminals at the dIPN and was not observed in the soma of dHb neurons (Figure 1F). Indeed, analysis of different dHb focal planes in multiple explants failed to reveal neuronal cell bodies exhibiting negatively correlated calcium signals during spontaneous activity (Figures 1C–1E and S1). The results indicate that calcium signals in dHb soma are not always reflective of the calcium dynamics at their terminals.

Calcium signaling data also revealed a local negative interaction between dHb terminals at the IPN. We analyzed activity in dHb terminals throughout the IPN (Video S3). By applying *k*-means clustering and manual inspection of the calcium signals, we identified five spatially segregated domains of axon terminals with distinct patterns of activity: (1) dIPN showing mainly calcium inhibition with few calcium bursts (red); (2) dorsal half of the vIPN (dvIPN) displaying frequent calcium bursts of low and high amplitude, with the high-amplitude bursts followed by calcium inhibition (gray); (3) ventral half of the vIPN (vvIPN), showing high-amplitude calcium bursts followed by inhibition (blue); (4) caudal area of the vIPN (cvIPN) (magenta), which clustered together with the dIPN exhibiting calcium inhibition; and (5) raphe area exhibiting calcium bursts without inhibition (green; Figures 1J–1P).

Notably, terminals at the dIPN and raphe exhibited negatively correlated calcium signals (Figure 1L), which we refer to as negatively correlated events. Calcium inhibition only occurred in terminals at the dIPN when high-amplitude bursts were observed at the vvIPN and raphe (Figure 1N), but not when calcium bursts were restricted to the dvIPN (Figure 1O). This suggests that dHb neurons that target the dvIPN differ from those innervating the vvIPN and raphe. Moreover, prior to or following a negatively correlated event, terminals at the dIPN showed higher GCaMP signals compared to those observed in the vIPN (Figures 1K,

(E, I, and P) Average  $\Delta F/F$  traces (black) of individual calcium events (gray).

(E) Traces of green and blue neurons exhibiting synchronized activity. *n* = 6 explants, 29 events. See Video S1.

(I) Traces of calcium bursts in the ventral dHb and dHb terminals at the vIPN and raphe (green and blue). Note that dHb terminals at the dIPN exhibit inhibition (trace 4). *n* = 5 explants, 24 events. See Video S2.

(P) Traces of negatively correlated events in dHb terminals at the IPN and raphe. *n* = 6 explants, 35 calcium events. See Video S3.

(K) Lateral view of dHb terminals expressing GCaMP7a at the IPN and raphe (green arrowheads) before and during a calcium burst event.

(N and O) Single-frame images showing calcium signal changes. Blue (N) and green (O) boxed events in (M) are shown. Areas with increased (white) or decreased (green) signals are outlined (dotted lines). Right panels show traces in the IPN and raphe during the calcium event on left. *n* = 21/23 explants show similar calcium signaling domains.

Scale bars: 20  $\mu$ m (B and J) or 50  $\mu$ m (F). See also Figures S1–S4.



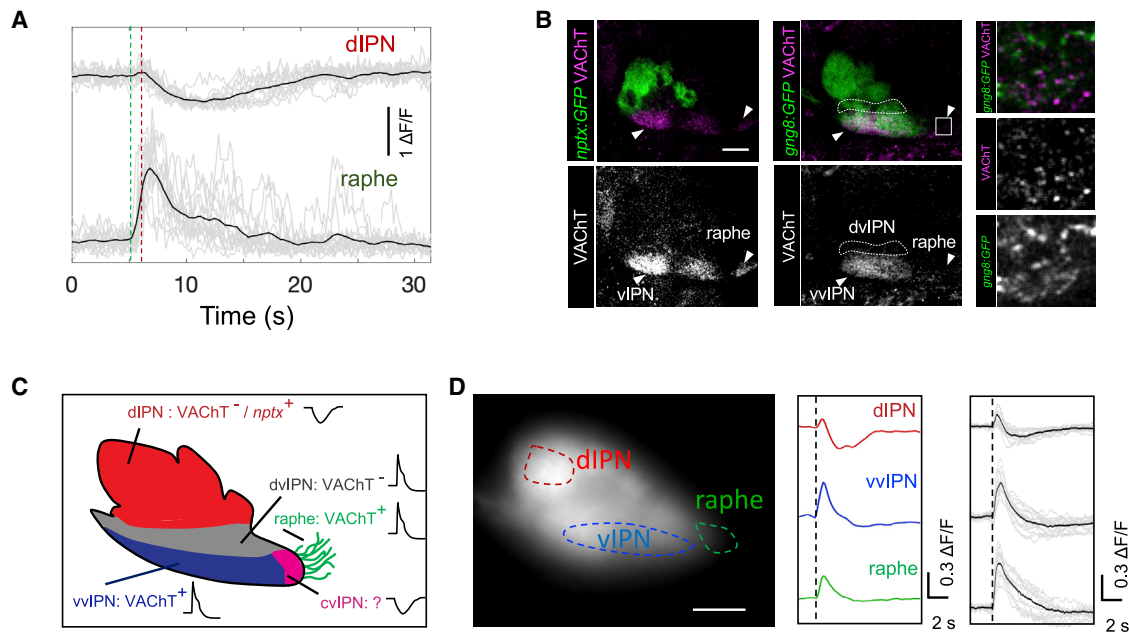


**Figure 2. Synchronized cholinergic terminal activity at vIPN/raphe precedes non-cholinergic terminal inhibition at dIPN**

(A) Average  $\Delta F/F$  trace (black) of negatively correlated events (gray) in dHb terminals at the dIPN (top) and raphe (bottom). Time of increase (green) and inhibition (red) is indicated (dotted lines). Note the delay between the two events ( $931 \pm 50$  ms;  $n = 5$  explants, 62 events).

(B) Sagittal sections of anti-GFP (green) and anti-VAcHT (magenta) labeling in 6 dpf *Tg(nptx2:Gal4-VP16)<sup>rw0143a</sup>;Tg(UAS:GFP)<sup>c426</sup>* (left) and *Tg(gng8:GAL4ff)<sup>c426</sup>;Tg(UAS:GFP)<sup>c426</sup>* (middle) larvae. White arrowheads indicate VAcHT labeling in vvIPN and raphe. White box (middle) corresponds to magnified panels on right. Scale bar: 20  $\mu$ m.

(C) Summary of dHb terminal domains. *nptx:Gal4;UAS:GFP*-positive dIPN domain is indicated (*nptx<sup>+</sup>*). The cvIPN is only identified based on calcium signals. Calcium bursts and inhibition are labeled with graph plots.

(D) Electric shock induces negatively correlated events. (Left) Lateral view of *Tg(gng8:GAL4ff)<sup>c426</sup>;Tg(UAS:GCaMP7a)* larva expressing GCaMP in dHb terminals is shown. dIPN, vIPN, and raphe are outlined (dotted lines). (Middle) Representative  $\Delta F/F$  traces upon electric shock (black dotted line) are shown. (Right) Average traces (black) of calcium events (gray) after electric shock are shown ( $n = 8$  larvae, 16 events). Scale bar represents 20  $\mu$ m.

1N, S2A, and S2B). The higher signals were not merely due to greater terminal density at the dIPN relative to the vIPN because we found no difference in the ratio of axon terminals in the two regions when labeled with GFP (Figures S2A' and S2B).

Quantification of calcium signaling kinetics revealed that the time to reach maximum amplitude (peak time) occurred earlier in terminals at the vvIPN compared to the raphe ( $1.13 \pm 0.42$  s versus  $1.59 \pm 0.72$  s), and the duration at half peak time (half duration) of the calcium burst was shorter ( $2.72 \pm 0.56$  s versus  $3.64 \pm 1.55$  s; Figures S3A–S3C). Peak inhibition in terminals at the dIPN occurred later ( $4.33 \pm 1.4$  s) and lasted longer ( $9.2 \pm 2.9$  s) than the calcium bursts (Figures S3D and S3E). Activation at the vvIPN was followed by a period of inhibition not observed in terminals at the raphe. Therefore, to resolve the relationship between the negatively correlated events, we measured activity in terminals at the dIPN and at the raphe as a proxy for the vvIPN. We found a  $931 \pm 50$  ms delay between the onset of the calcium burst and inhibition (Figure 2A), suggesting that calcium activity at the vvIPN triggers calcium inhibition in the dIPN.

To identify the neurotransmitter phenotype of neurons that exhibit calcium bursts at the vvIPN and raphe, we assessed vesicular acetylcholine transporter (VAcHT) expression by immunolabeling in *Tg(nptx2:Gal4-VP16)<sup>rw0143a</sup>;Tg(UAS:GFP)<sup>c354</sup>* larvae. We previously found that this transgenic line mainly labels non-cholinergic neurons in the left dHb and their projections to

the dIPN.<sup>12</sup> We confirmed that GFP expression does not colocalize with VAcHT protein (Figure 2B), whereas dHb terminals at the vvIPN and raphe are positive for VAcHT staining in *TgBAC(gng8:GAL4ff)<sup>c426</sup>;Tg(UAS:GFP)<sup>c354</sup>* larvae (Figure 2B). We therefore conclude that calcium bursts at these regions are due to the synchronized activation of dHb cholinergic neurons (Figure 2C). Negatively correlated events are already apparent in 3-day-old larvae (Figure S4) upon emergence of spontaneous activity in dHb neurons (data not shown), suggesting that it is a hardwired mode of activity, coincident with establishment of the dHb-IPN pathway.

To determine whether external stimuli provoke negatively correlated events *in vivo*, we applied a mild electric shock to larvae. Indeed, we observed negatively correlated events between dHb terminals at the dIPN and vIPN/raphe (Figure 2D). However, due to tissues surrounding the brain, the resolution of calcium activity was inferior in larvae compared with the brain explants. Nevertheless, this result indicates that negatively correlated events can be induced *in vivo*, suggesting it is a physiologically relevant mode of neuronal activation.

#### Nicotinic acetylcholine receptors do not mediate negatively correlated events

The MHB/dHb-IPN pathway shows the highest expression and greatest variety of nicotinic acetylcholine receptor

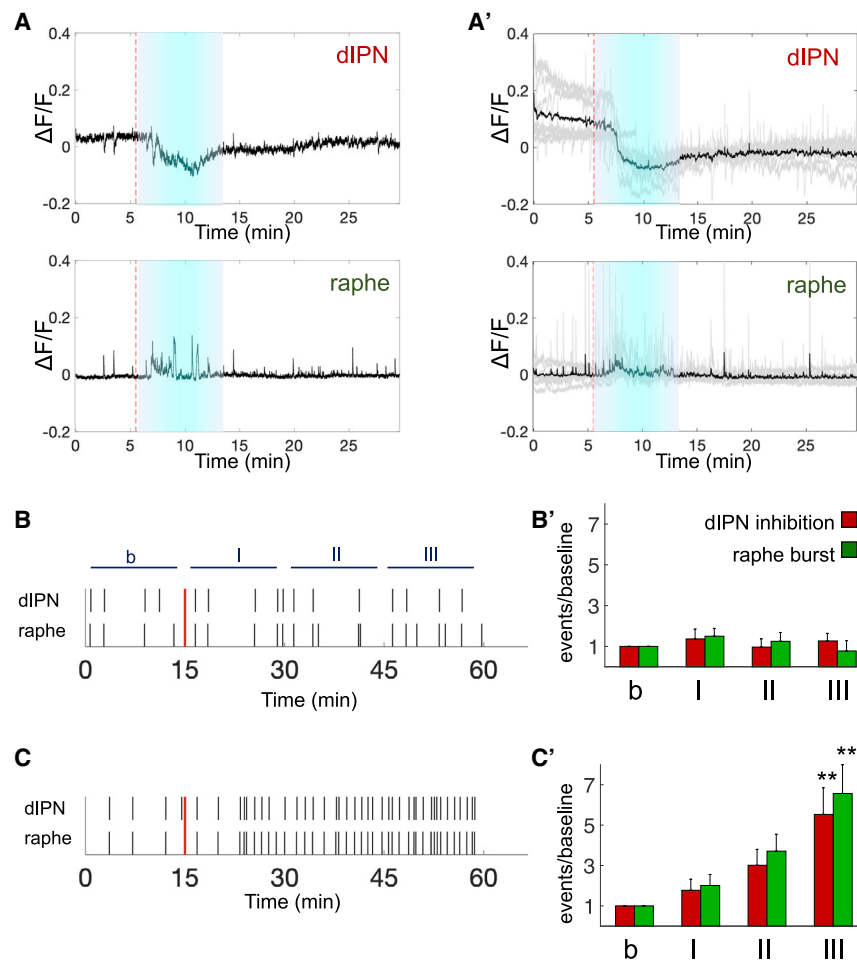


**Figure 3. Nicotine induces prolonged negatively correlated event**

(A) Representative  $\Delta F/F$  traces from dHb terminals in *Tg(gng8:GAL4ff)<sup>c426</sup>;Tg(UAS:GCaMP7a)* explant. 5 min nicotine (10  $\mu\text{M}$ ) perfusion induces inhibition at the dIPN (top) and bursts at the raphe (bottom).

(A') Average  $\Delta F/F$  traces (black) of nicotine-induced negatively correlated events (gray). Duration (cyan boxes) and initiation (red dotted lines) of nicotine application are indicated.  $n = 8$  explants.

(B and C) Representative raster plots of dIPN inhibition and raphe burst events. (B) Control and (C) nAChR antagonist (100  $\mu\text{M}$  mecamylamine and 10  $\mu\text{M}$  d-tubocurarine) application are shown. Introduction of E3 solution (B) or antagonists (C) are indicated (red lines).

(B' and C') Ratio of average number of events in 15-min windows (I–III) and baseline activity (b) after applying (B') E3 ( $n = 4$ ) or (C') antagonists ( $n = 6$ ). Bars indicate negatively correlated events in dHb terminals at the raphe (green, bursts) and dIPN (red, inhibition). One-way ANOVA followed by Tukey's test; \*\* $p < 0.005$ . b, 15 min of baseline; I, 0–15 min after application; II, 15–30 min after application; III, 30–45 min after application.

(nAChR) subunits in the brain.<sup>17</sup> Because calcium inhibition in non-cholinergic dHb terminals is preceded by a calcium burst in cholinergic terminals, we investigated whether inhibition depends on the activation of nAChRs.<sup>9</sup> Perfusion of nicotine resulted in prolonged calcium inhibition of dHb terminals at the dIPN, which corresponded with an extended series of calcium bursts in dHb terminals at the raphe (Figures 3 A and 3A';  $260 \pm 176$  s). To determine the contribution of nAChRs in the generation of negatively correlated events, we administered mecamylamine and d-tubocurarine, effective blockers of cholinergic transmission in the larval IPN.<sup>9</sup> nAChRs antagonists did not attenuate but rather increased the frequency of negatively correlated events (Figures 3 B–3C'). Thus, activation of nAChRs is not required for negatively correlated events between cholinergic and non-cholinergic dHb terminals at the IPN.

#### dHb terminal calcium bursts correlate with GABAergic currents in IPN neurons

To understand the basis for negatively correlated events, we combined calcium imaging of dHb terminals with patch-clamp recordings of neurons at the interface between the dIPN and vIPN. Recording at  $-60$  mV (equilibrium potential of  $\text{Cl}^-$  ions) revealed that calcium bursts correlated with a barrage of

GABAergic inhibitory postsynaptic currents. The cholinergic/glutamatergic postsynaptic barrage was relatively short (half-duration =  $262 \pm 124$  ms) and synchronized with the onset of the calcium burst (delay =  $67 \pm 69$  ms). In contrast, the barrage of GABAergic synaptic currents had a delayed onset (delay =  $162 \pm 80$  ms) and lasted longer (half-duration =  $387 \pm 143$  ms). These results suggest that calcium bursts correspond to the release of glutamate and acetylcholine from dHb terminals at the IPN, which is followed by local release of GABA from IPN neurons.

#### Presynaptic GABA<sub>B</sub> receptors in dHb axon terminals mediate calcium inhibition

GABA has an inhibitory presynaptic action on transmitter release through metabotropic GABA<sub>B</sub> receptors.<sup>18</sup> We asked whether GABA released by the IPN could activate presynaptic metabotropic GABA<sub>B</sub> receptors, thereby repressing dHb terminal activity. Application of cgp55845, a GABA<sub>B</sub> receptor antagonist, resulted in a  $74\% \pm 9\%$  reduction in the amplitude of calcium inhibition ( $-0.16 \pm 0.03$  versus  $-0.04 \pm 0.01$ ) without affecting the amplitude of calcium bursts ( $0.22 \pm 0.09$  versus  $0.26 \pm 0.13$ ; Figures 5A and 5A'). To test the role of GABA<sub>B</sub> receptors directly, we applied tetrodotoxin to inhibit the propagation of action potentials and eliminate all negatively correlated events. We

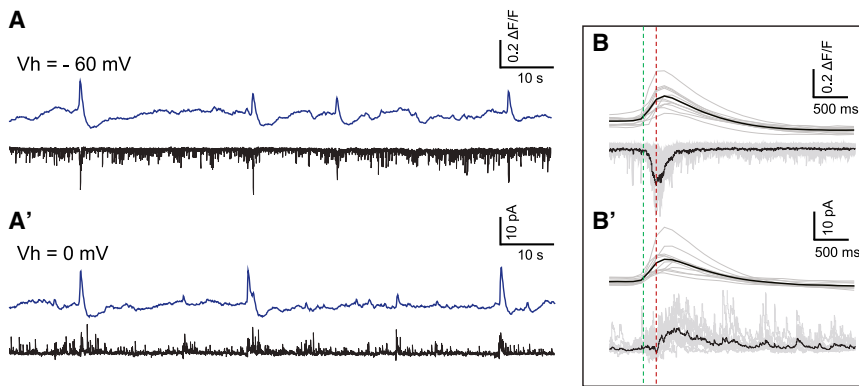


**Figure 4. Calcium bursts correspond to acetylcholine/glutamate and GABAergic currents**

(A and A')  $\Delta F/F$  traces of dHb terminals (blue) aligned with simultaneous patch-clamp recording of IPN neurons (black) show correlation of calcium bursts with increase in glutamatergic/cholinergic inward currents (A;  $V_h = -60$  mV) and GABAergic outward currents (A';  $V_h = 0$  mV).

(B and B') Average traces (black) of calcium bursts (top) aligned with synaptic responses (bottom) at holding potentials of  $-60$  mV (B;  $n = 4$  explants, 42 events) and  $0$  mV (B';  $n = 3$  explants, 23 events). Dotted lines indicate onset for inward (green) and outward (red) currents.

then administered baclofen, a GABA<sub>B</sub> receptor agonist, and observed a prolonged decrease in the calcium baseline, similar in amplitude to that observed during inhibition of dHb terminals at the dIPN (Figures 5B and 5B'). Calcium imaging of dHb terminals together with patch-clamp recordings of IPN neurons confirmed that prolonged inhibition corresponds with a decrease in the frequency of fast postsynaptic inward currents recorded in IPN neurons (Figures 5C and 5C').

In zebrafish, there are two GABA<sub>B</sub>1 receptor genes, *GABA<sub>B</sub> receptor 1a* (*gabbr1a*) and *1b* (*gabbr1b*).<sup>19</sup> We found that *gabbr1a*, but not *gabbr1b*, is prominently expressed in the dHb in a larger domain of the left nucleus compared with the right, in the location of non-cholinergic neurons (Figures 5D and 5E). Strikingly, *gabbr1a* transcripts localized to the dHb nuclei and were not detected in other brain regions, including the IPN (Figure 5D). Together, these results suggest that calcium inhibition is due to the activation of presynaptic GABA<sub>B</sub> receptors in non-cholinergic terminals at the dIPN.

### Retrograde signaling from GABAergic IPN neurons to non-cholinergic habenular inputs

To determine that inhibition of dHb terminals at the dIPN results from GABA released upon IPN activation, we carried out electrical stimulation of the IPN with calcium imaging (Figure 6A; Video S4). Activation of the IPN effectively triggered negatively correlated events consisting of the vIPN/raphe calcium burst (likely due to the activation of the dHb terminals at the vIPN) and dIPN calcium inhibition (Figure 6B). We next perfused a GABA<sub>B</sub> antagonist, cgp55845, during negatively correlated events induced by electrical stimulation and found a  $90\% \pm 13\%$  decrease in calcium inhibition at the dIPN ( $-0.15 \pm 0.07$  versus  $-0.02 \pm 0.02$ ) without any change in calcium bursts at the raphe ( $0.22 \pm 0.08$  versus  $0.2 \pm 0.06$ ; Figures 6B–6E).

To verify the presence of GABAergic neurons in the IPN, we imaged the *TgBAC(gng8:GAL4ff)<sup>c426</sup>;Tg(UAS:GFP)<sup>c426</sup>;Tg(gad1b:|R|-GFP)* larvae in which dHb terminals are labeled with GFP and GABAergic neurons by RFP.<sup>20</sup> We found that nearly half of IPN neurons were labeled by *gad1b:RFP* ( $48\% \pm 2\%$ ;  $n = 3$  larvae;  $N = 479$  cells; Figure 6F), with more located in the dIPN than vIPN ( $79\% \pm 11\%$  versus  $21\% \pm 11\%$ ;  $n = 3$  larvae;  $N = 232$  *gad1b:RFP*<sup>+</sup> cells). These results suggest that a higher concentration of GABA is released from neurons in the dIPN.

## DISCUSSION

The dHb of zebrafish larvae respond to external factors, including light, odor, and aversive stimuli.<sup>6,14,15</sup> A prerequisite to investigating the innate hardwired activity of the dHb-IPN pathway was eliminating the influence of external factors. We achieved this by performing calcium imaging using a whole brain explant preparation, in which central neural circuits, including the dHb-IPN pathway, remain intact. We found a stereotyped mode of spontaneous activity in dHb soma and axon terminals at the IPN.

Through pharmacological and electrophysiological manipulations, we determined that synchronized activation of dHb cholinergic neurons inhibit non-cholinergic neurons by an atypical mechanism of target-mediated, trans-inhibition at the level of axon terminals.

### Negatively correlated events at axon terminals of cholinergic and non-cholinergic dHb neurons

Clustering algorithms are commonly used to segregate neurons into different functional groups during calcium imaging of neuronal soma.<sup>21–23</sup> The  $k$  value and threshold for hierarchical clustering were determined from a previous study of the zebrafish dHb<sup>23</sup> and manual inspection of the activity of individual neurons assigned to different clusters. We obtained similar, but not identical, results from  $k$ -means and hierarchical clustering methods. Nevertheless, the minor difference resulting from the clustering algorithms does not alter the conclusion showing that most dHb neurons on the right and a small cluster on the left show high levels of synchronized spontaneous activity. The location of these neurons corresponds to different neurotransmitter phenotypes: cholinergic and somatostatin,<sup>12</sup> suggesting that dHb neurons expressing the same neurotransmitter function together.

In analyzing group dynamics of axon terminals, we found it important to also carry out manual inspection of raw data. For example, only calcium peaks at the vIPN and not the dIPN correlated with dIPN inhibition. VACHT antibody labeling in transgenic lines confirmed that cholinergic dHb terminals innervate only the vIPN, indicating that the dIPN is innervated by different types of neurons. In addition, a small domain in the caudal vIPN clustered together with the terminals at the dIPN. Although there are currently no available molecular markers to differentiate between the dHb axon terminals at the cvIPN and dIPN, spatial segregation between the two areas suggests that

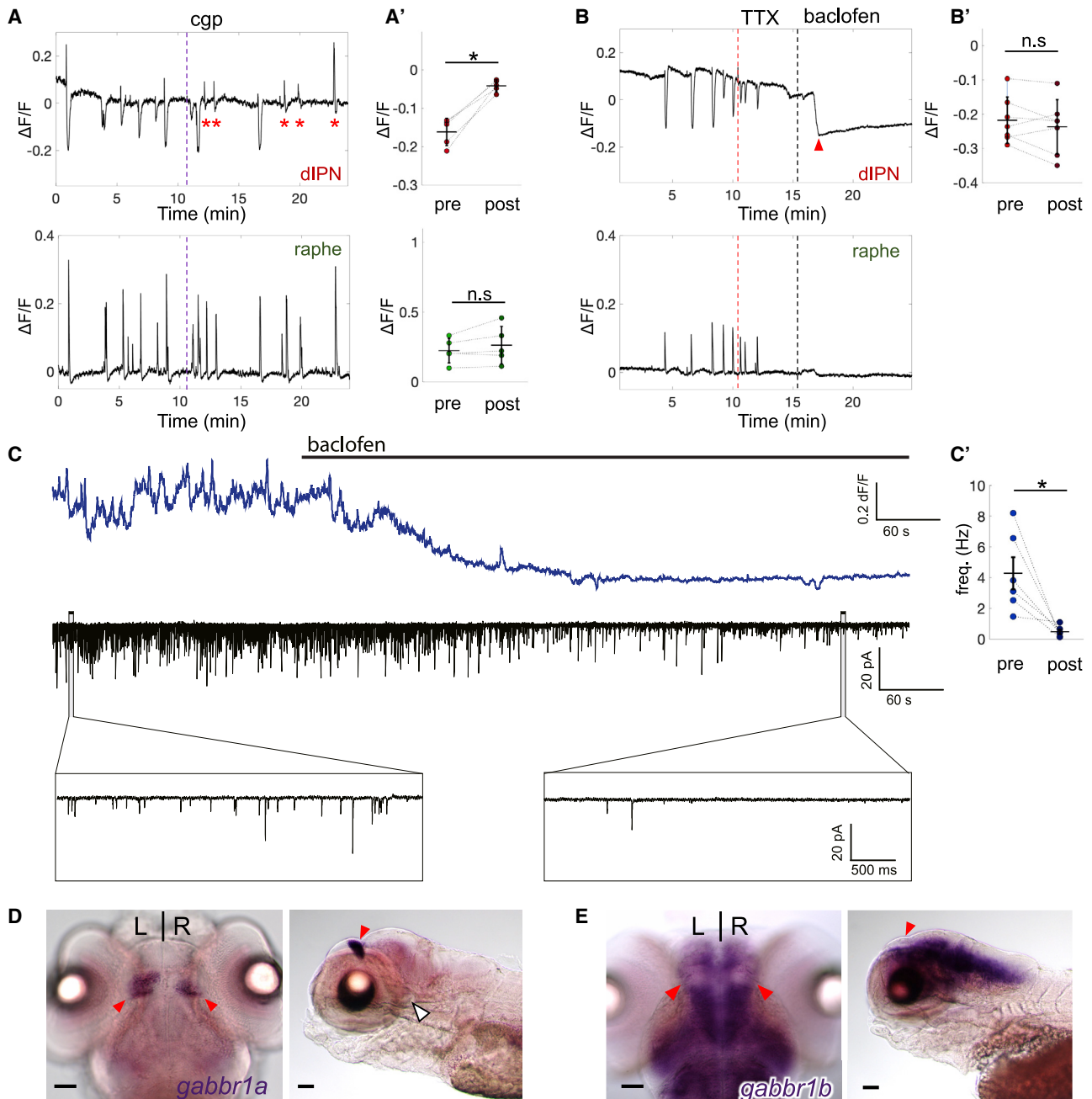


**Figure 5. Calcium inhibition occurs via presynaptic GABA<sub>B</sub> receptors**

(A and B) Representative  $\Delta F/F$  traces in terminals at dIPN (top) and raphe (bottom) after application of (A) 1  $\mu$ M *cgp55845* or (B) 3  $\mu$ M tetrodotoxin (TTX) + 2  $\mu$ M baclofen. Time of drug application is indicated (vertical lines).

(A') Average peak amplitude before and after *cgp55845* application in terminals at the dIPN ( $-0.16 \pm 0.03$  versus  $-0.04 \pm 0.01$ ) and raphe ( $0.22 \pm 0.09$  versus  $0.26 \pm 0.13$ ) during inhibition (top) and burst (bottom).  $n = 6$  explants, 50 events. Red asterisks indicate attenuated calcium inhibition at the dIPN after *cgp55845* application.

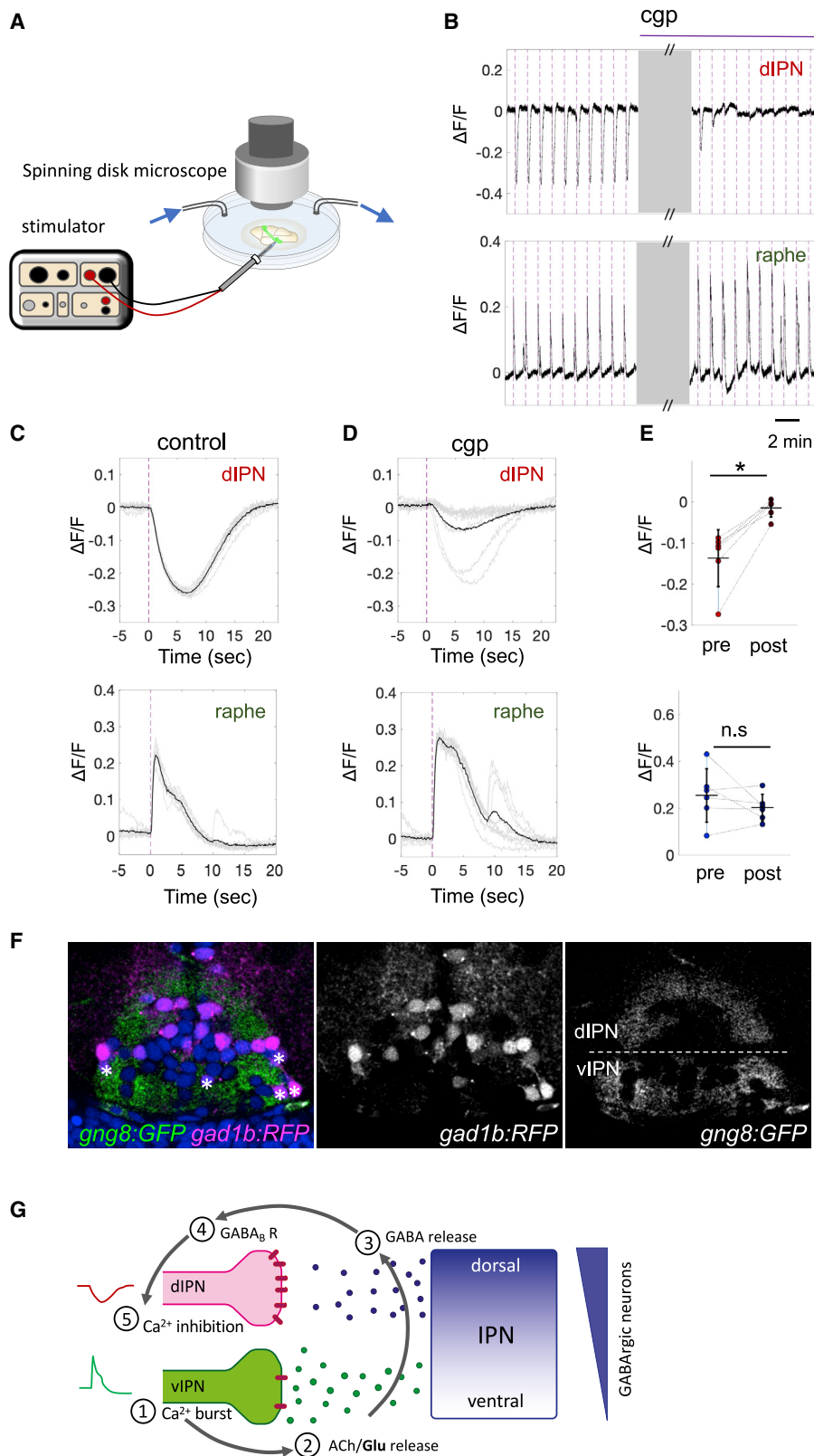
(B') Paired plots comparing average inhibition amplitude in control conditions ( $-0.22 \pm 0.07$ ) to the average baseline decrease after baclofen application ( $-0.24 \pm 0.08$ ).  $n = 7$  explants, 46 events. Note abrupt decrease (red arrowhead) in baseline at the dIPN following baclofen.

(C)  $\Delta F/F$  traces of IPN (top) aligned with simultaneous whole-cell, patch-clamp recording trace (middle) upon baclofen perfusion. Time of baclofen application is indicated (black bar). Magnified traces of synaptic activity before (left) and after (right) baclofen (bottom panels) are shown.

(C') Paired plot of synaptic activity frequency before ( $4.29 \pm 1.05$  Hz) and after ( $0.47 \pm 0.15$  Hz) baclofen.  $n = 6$  explants. Mean  $\pm$  SD is indicated in (A'), (B'), and (C'). Wilcoxon signed-rank test. \* $p < 0.05$ .

(D and E) Dorsal (left) and sagittal (right) views of *gabbr1a* (D) and *gabbr1b* (E) expression at 6 dpf. dHb nuclei (red arrowheads) and absence of expression at IPN (white arrowhead; D) are shown. Scale bars: 50  $\mu$ m.





(legend on next page)

they are targeted by different dHb neurons. In conclusion, cholinergic neurons exhibit synchronized activity and project to the vVIPN and raphe, which display negatively correlated events with axon terminals at the dIPN (Figure 2C).

### Nicotine promotes negatively correlated events in the dHb-IPN pathway

We found that nicotine induces prolonged duration of the negatively correlated event. We previously showed that a cocktail of nAChR antagonists inhibits approximately 80% of cholinergic currents in IPN neurons.<sup>9</sup> However, application of antagonists failed to attenuate but rather increased the frequency of negatively correlated events. The cholinergic system can increase the excitability of GABAergic interneurons in the neocortex and the lateral habenula.<sup>24,25</sup> Likewise, our data suggest that GABAergic neurons are activated by nAChRs in the IPN. We hypothesize that blocking nAChRs throughout the whole brain inhibits GABAergic signaling, resulting in a global increase in synchronized network activity.

Although nAChR activation can generate a negatively correlated event, the release of GABA from IPN neurons to induce inhibition is predominantly triggered by glutamatergic rather than cholinergic transmission from the dHb terminals at the IPN during spontaneous activity,

### Localization of the GABA<sub>B</sub> receptor to non-cholinergic terminals at the dIPN mediates presynaptic inhibition

We found that *gabbr1a* is expressed asymmetrically in a large area in the left and smaller area in the right dHb, indicating that the GABA<sub>B</sub> receptor is present in non-cholinergic neurons that innervate the dIPN in larvae. Moreover, *gad1b*-positive neurons predominate in the dIPN, suggesting that GABA released from dIPN neurons activates presynaptic GABA<sub>B</sub> receptors on non-cholinergic terminals at the dIPN. Based on calcium imaging, pharmacology, electrical stimulation, and molecular studies, we propose a model whereby (1) activation of cholinergic dHb neurons (2) activates GABAergic neurons in the IPN, resulting in the (3) release of GABA that through retrograde signaling (4) activates inhibitory presynaptic GABA<sub>B</sub> receptors on non-cholinergic dHb terminals at the dIPN, leading to (5) inhibition of glutamatergic transmission (Figure 6G).

How does activation of vVIPN neurons induce GABA release by dIPN neurons? Single cell labeling experiments showed the diverse morphology of IPN neurons, including those that appear to be interneurons extending their processes between the dorsal and vIPN.<sup>26</sup> We hypothesize that communication between vVIPN and dIPN neurons could be mediated by such interneurons

connecting the dorsal and ventral IPN. Another possibility is that more vVIPN neurons are GABAergic than visualized by the transgenic line used in this study, akin to what has been shown for the adult IPN.<sup>27</sup> Thus, GABAergic vVIPN neurons might form direct synaptic connections or, through non-synaptic volume transmission, release GABA to inhibit non-cholinergic terminal activity at the dIPN.

As the MHB/dHb-IPN pathway is evolutionarily conserved in all vertebrates,<sup>9,28</sup> it is likely that this mode of hardwired activity is not unique to zebrafish. Indeed, a recent study on mice reports that presynaptic GABA<sub>B</sub> receptors at non-cholinergic terminals at the IPN play an inhibitory role on plasticity,<sup>29</sup> suggesting a conserved role for these receptors.

### Model for competitive selection between dHb circuits on behavior

It is crucial for an animal to identify the most salient stimulus among many concurrent external stimuli and select a single behavioral response. One example is the flight, freeze, or fight response.<sup>30</sup> During early stages of development, hardwired circuits to execute specific behavioral repertoires, such as escape (flight), are essential for survival.<sup>31</sup> The process of transforming multiple sensory inputs into a single behavioral outcome is termed competitive selection and includes selective attention and decision making.<sup>32</sup> Computational formulations, such as winner-take-all models, have been proposed,<sup>33,34</sup> and recent studies have begun to elucidate the mechanisms for behavioral selection in competing circuits.<sup>35–38</sup>

Higher baseline GCaMP fluorescence in the terminals at the dIPN relative to the vIPN suggests that non-cholinergic neurons display high-frequency oscillation.<sup>39</sup> We propose that the synchronized burst in cholinergic terminals at the vIPN transiently inhibits this constitutive activity that occurs in non-cholinergic neurons, ensuring only one pathway is active at any given time.

What could be the advantage of having local inhibition at the terminal level? Different external stimuli preferentially activate left or right dHb neurons.<sup>6,14,15</sup> However, the ratio of asymmetric dHb activation depends on the intensity of the stimulus for both light and electric shock (personal observations), suggesting that the left and right dHb can be co-activated by the same stimulus. We suspect that this setup of local inhibition would ensure that (1) only one circuit is active at a time and, (2) upon exposure to multiple stimuli, a hierarchy is established between the stimuli.

Aversive behavior refers to emotional states with negative valence, such as fear or anxiety. Fear is defined as a response to a factual known threat while anxiety as an unknown, poorly defined threat. Brain areas that contribute to fear and anxiety

### Figure 6. Direct stimulation of IPN induces GABA<sub>B</sub>-receptor-mediated inhibition in terminals at the dIPN

(A) Schematic of setup for simultaneous electrical stimulation and drug perfusion.

(B) Representative  $\Delta F/F$  traces showing attenuation of dIPN inhibition by electrical stimulation after *cgp55845* perfusion (top), with bursts unaffected in the raphe (bottom). Gray boxes represent 10 min after *cgp55845* application. See also Video S4.

(C and D) Average traces (black) of calcium events (gray, 10 stimuli) before (C) and after (D) *cgp55845*.

(E) Paired plot of average peak amplitudes before and after *cgp55845* application during inhibition (top;  $-0.15 \pm 0.07$  versus  $-0.02 \pm 0.02$ ) and burst (bottom;  $0.22 \pm 0.08$  versus  $0.2 \pm 0.06$ ).  $n = 6$  explants, 71 events. Purple dotted lines indicate time of electrical stimulation (B–D). Purple line in (B) denotes duration of *cgp55845* application. Wilcoxon signed-rank test; \* $p < 0.05$ ; n.s., not significant. Mean  $\pm$  SD indicated.

(F) Transverse section of *Tg(gng8:GAL4ff)<sup>C426</sup>; Tg(UAS:GFP)<sup>C426</sup>; Tg(gad1b:|R|-GFP)* larval IPN surrounded by dHb terminals (green) and GABAergic neurons (magenta). Hoechst nuclear staining (blue) is shown. White asterisks indicate *gad1b:RFP+* neurons in vIPN. White dotted line separates dIPN and vIPN (right panel).

(G) Model illustrating the mechanism underlying negatively correlated events in dHb terminals at the IPN (see Discussion).

exhibit great overlap, including the amygdala, medial prefrontal cortex, and the hippocampus.<sup>40</sup> Although recent optogenetic and *in vivo* studies have begun unraveling the microcircuits that participate in these behaviors,<sup>35,41</sup> how they interact with other areas of the brain is unclear. The highly conserved MHb/dHb-IPN pathway consists of two circuits composed of different neuronal populations, which mediate fear- or anxiety-related behaviors.<sup>3–5,16</sup> We propose that the trans-inhibition mechanism between cholinergic and non-cholinergic dHb-IPN circuits underlies competitive selection of aversive behavioral responses.

A brief electric shock induces fast swim followed by freezing behavior before returning to baseline locomotion in larval zebrafish.<sup>6</sup> Here, we demonstrate that it can also promote negatively correlated events in the dHb terminals at the IPN. We hypothesize that activation of the cholinergic pathway by electric shock results in a stereotypical fast swim (flight) response, which is followed by inhibition of the non-cholinergic pathway, allowing the animal to freeze. Prior to puberty, a flight or freeze response would be more beneficial than a fight response. In juveniles and adults, this dual circuit likely becomes more complex as different neuropeptides become expressed in the dHb-IPN pathway and with the maturation of behavioral repertoires from prior experience. For example, adult zebrafish exhibit a fight or flight response, manifested by a “winner” or “loser” phenotype in a social conflict paradigm, which is correlated with potentiation in non-cholinergic and cholinergic neuronal terminals, respectively.<sup>16</sup> We hypothesize that the “loser”/ flight behavior corresponds to the default response to an aversive stimulus upon activation of the cholinergic pathway. The “winner”/ fight behavior could result from preferential hyper-activation of the non-cholinergic pathway, corresponding to a heightened level of anxiety.

In conclusion, investigating neuronal population dynamics within an intact pathway has revealed an atypical mode of trans-inhibition between two excitatory neuronal populations at their axon terminals. This hardwired mode of competition could underlie the mechanism for competitive selection between these neural circuits and provide a physiological framework to explore the relationship between anxiety and fear.

## STAR★METHODS

Detailed methods are provided in the online version of this paper and include the following:

- KEY RESOURCES TABLE
- RESOURCE AVAILABILITY
  - Lead contact
  - Material availability
  - Data and code availability
- EXPERIMENTAL MODEL AND SUBJECT DETAILS
- METHOD DETAILS
  - Explant Dissection
  - Pharmacology
  - Calcium Imaging
  - Patch-clamp recordings and simultaneous Ca<sup>2+</sup> imaging
  - Immunohistochemistry
  - RNA *in situ* Hybridization

- Electrical shock assay
- Electrical stimulation
- QUANTIFICATION AND STATISTICAL ANALYSIS
  - Calcium data analysis
  - Statistical analysis

## SUPPLEMENTAL INFORMATION

Supplemental information can be found online at <https://doi.org/10.1016/j.cub.2021.08.051>.

## ACKNOWLEDGMENTS

We thank Hitoshi Okamoto for insightful feedback on this project, Marco Diana and Nathalie Leresche for advice on pharmacology experiments, Eric Schwartz and Soumaya Imarraine for helpful comments on the manuscript, Jean-Pierre Coutanceau for aid in zebrafish husbandry, and the IBPS aquatic animal facility and imaging facility. Hitoshi Okamoto, Koichi Kawakami, and Shin-ichi Higashijima provided the *Tg(nptx2:Gal4-VP16)<sup>rw0143a</sup>*, *Tg(UAS:G-CaMP7a)*, and *Tg(gad1b:|R|-GFP)* lines. This study was supported by a graduate fellowship from the Alexis and Anne Marie Habib Foundation (to M.A.Y.), NIH grant R37HD091280 (to M.E.H.), and the ATIP-Avenir young investigator grant (INSERM/CNRS) and Emergence grant (Sorbonne Université; to E.H.).

## AUTHOR CONTRIBUTIONS

M.Z., S.W., R.C., E.R.D., P.L., M.E.H., J.-M.M., and E.H. designed experiments. M.Z., E.B., M.A.Y., S.M.A.N., H.L.C., S.W., R.C., E.R.D., J.-M.M., and E.H. conducted the experiments. M.Z., S.M.A.N., S.W., H.S., J.-M.M., and E.H. analyzed data. E.H. wrote the manuscript with input from all authors.

## DECLARATION OF INTERESTS

The authors declare no competing interests.

Received: April 22, 2021

Revised: July 12, 2021

Accepted: August 18, 2021

Published: September 15, 2021

## REFERENCES

1. McLaughlin, I., Dani, J.A., and De Biasi, M. (2017). The medial habenula and interpeduncular nucleus circuitry is critical in addiction, anxiety, and mood regulation. *J. Neurochem.* 142 (Suppl 2), 130–143.
2. Fakhoury, M. (2018). The dorsal diencephalic conduction system in reward processing: Spotlight on the anatomy and functions of the habenular complex. *Behav. Brain Res.* 348, 115–126.
3. Yamaguchi, T., Danjo, T., Pastan, I., Hikida, T., and Nakanishi, S. (2013). Distinct roles of segregated transmission of the septo-habenular pathway in anxiety and fear. *Neuron* 78, 537–544.
4. Seigneur, E., Polepalli, J.S., and Südhof, T.C. (2018). *Cbln2* and *Cbln4* are expressed in distinct medial habenula-interpeduncular projections and contribute to different behavioral outputs. *Proc. Natl. Acad. Sci. USA* 115, E10235–E10244.
5. Agetsuma, M., Aizawa, H., Aoki, T., Nakayama, R., Takahoko, M., Goto, M., Sassa, T., Amo, R., Shiraki, T., Kawakami, K., et al. (2010). The habenula is crucial for experience-dependent modification of fear responses in zebrafish. *Nat. Neurosci.* 13, 1354–1356.
6. Duboué, E.R., Hong, E., Eldred, K.C., and Halpern, M.E. (2017). Left habenular activity attenuates fear responses in larval zebrafish. *Curr. Biol.* 27, 2154–2162.e3.
7. Cuello, A.C., Emson, P.C., Paxinos, G., and Jessell, T. (1978). Substance P containing and cholinergic projections from the habenula. *Brain Res.* 149, 413–429.

8. Kadar, T., Silbermann, M., Steinhagen-Thiessen, E., and Levy, A. (1989). Age-related changes in the cholinergic components within the central nervous system of CW1 female mice. I. Structural analysis. *Mech. Ageing Dev.* **47**, 133–144.
9. Hong, E., Santhakumar, K., Akitake, C.A., Ahn, S.J., Thisse, C., Thisse, B., Wyart, C., Mangin, J.-M., and Halpern, M.E. (2013). Cholinergic left-right asymmetry in the habenulo-interpeduncular pathway. *Proc. Natl. Acad. Sci. USA* **110**, 21171–21176.
10. Aizawa, H., Bianco, I.H., Hamaoka, T., Miyashita, T., Uemura, O., Concha, M.L., Russell, C., Wilson, S.W., and Okamoto, H. (2005). Laterotopic representation of left-right information onto the dorso-ventral axis of a zebrafish midbrain target nucleus. *Curr. Biol.* **15**, 238–243.
11. Gamse, J.T., Kuan, Y.S., Macurak, M., Brösamle, C., Thisse, B., Thisse, C., and Halpern, M.E. (2005). Directional asymmetry of the zebrafish epithalamus guides dorsoventral innervation of the midbrain target. *Development* **132**, 4869–4881.
12. deCarvalho, T.N., Subedi, A., Rock, J., Harfe, B.D., Thisse, C., Thisse, B., Halpern, M.E., and Hong, E. (2014). Neurotransmitter map of the asymmetric dorsal habenular nuclei of zebrafish. *Genesis* **52**, 636–655.
13. Otsu, Y., Lecca, S., Pietrajtis, K., Rousseau, C.V., Marcaggi, P., Dugué, G.P., Mailhes-Hamon, C., Mamei, M., and Diana, M.A. (2018). Functional principles of posterior septal inputs to the medial habenula. *Cell Rep.* **22**, 693–705.
14. Zhang, B.B., Yao, Y.Y., Zhang, H.F., Kawakami, K., and Du, J.L. (2017). Left habenula mediates light-preference behavior in zebrafish via an asymmetrical visual pathway. *Neuron* **93**, 914–928.e4.
15. Dreosti, E., Vendrell Llopis, N., Carl, M., Yaksi, E., and Wilson, S.W. (2014). Left-right asymmetry is required for the habenulae to respond to both visual and olfactory stimuli. *Curr. Biol.* **24**, 440–445.
16. Chou, M.-Y., Amo, R., Kinoshita, M., Cherng, B.-W., Shimazaki, H., Agetsuma, M., Shiraki, T., Aoki, T., Takahoko, M., Yamazaki, M., et al. (2016). Social conflict resolution regulated by two dorsal habenular subregions in zebrafish. *Science* **352**, 87–90.
17. Antolin-Fontes, B., Ables, J.L., Görlich, A., and Ibañez-Tallon, I. (2015). The habenulo-interpeduncular pathway in nicotine aversion and withdrawal. *Neuropharmacology* **96** (Pt B), 213–222.
18. Dutar, P., and Nicoll, R.A. (1988). A physiological role for GABAB receptors in the central nervous system. *Nature* **332**, 156–158.
19. Cocco, A., Rönnerberg, A.M.C., Jin, Z., André, G.I., Vossen, L.E., Bhandage, A.K., Thörnqvist, P.-O., Birnir, B., and Winberg, S. (2017). Characterization of the  $\gamma$ -aminobutyric acid signaling system in the zebrafish (*Danio rerio* Hamilton) central nervous system by reverse transcription-quantitative polymerase chain reaction. *Neuroscience* **343**, 300–321.
20. Satou, C., Kimura, Y., Hirata, H., Suster, M.L., Kawakami, K., and Higashijima, S. (2013). Transgenic tools to characterize neuronal properties of discrete populations of zebrafish neurons. *Development* **140**, 3927–3931.
21. Panier, T., Romano, S.A., Olive, R., Pietri, T., Sumbre, G., Candelier, R., and Debrégeas, G. (2013). Fast functional imaging of multiple brain regions in intact zebrafish larvae using selective plane illumination microscopy. *Front. Neural Circuits* **7**, 65.
22. Dunn, T.W., Mu, Y., Narayan, S., Randlett, O., Naumann, E.A., Yang, C.T., Schier, A.F.A., Freeman, J., Engert, F., and Ahrens, M.B.M.B. (2016). Brain-wide mapping of neural activity controlling zebrafish exploratory locomotion. *eLife* **5**, e12741.
23. Jetti, S.K., Vendrell-Llopis, N., and Yaksi, E. (2014). Spontaneous activity governs olfactory representations in spatially organized habenular microcircuits. *Curr. Biol.* **24**, 434–439.
24. Picciotto, M.R., Higley, M.J., and Mineur, Y.S. (2012). Acetylcholine as a neuromodulator: cholinergic signaling shapes nervous system function and behavior. *Neuron* **76**, 116–129.
25. Jo, Y.H., and Role, L.W. (2002). Cholinergic modulation of purinergic and GABAergic co-transmission at in vitro hypothalamic synapses. *J. Neurophysiol.* **88**, 2501–2508.
26. Bianco, I.H., Carl, M., Russell, C., Clarke, J.D.W., and Wilson, S.W. (2008). Brain asymmetry is encoded at the level of axon terminal morphology. *Neural Dev.* **3**, 9.
27. Mueller, T., and Guo, S. (2009). The distribution of GAD67-mRNA in the adult zebrafish (teleost) forebrain reveals a prosomeric pattern and suggests previously unidentified homologies to tetrapods. *J. Comp. Neurol.* **516**, 553–568.
28. Ren, J., Qin, C., Hu, F., Tan, J., Qiu, L., Zhao, S., Feng, G., and Luo, M. (2011). Habenula “cholinergic” neurons co-release glutamate and acetylcholine and activate postsynaptic neurons via distinct transmission modes. *Neuron* **69**, 445–452.
29. Melani, R., Von Itter, R., Jing, D., Koppensteiner, P., and Ninan, I. (2019). Opposing effects of an atypical glycinergic and substance P transmission on interpeduncular nucleus plasticity. *Neuropsychopharmacology* **44**, 1828–1836.
30. Eilam, D. (2005). Die hard: a blend of freezing and fleeing as a dynamic defense - implications for the control of defensive behavior. *Neurosci. Biobehav. Rev.* **29**, 1181–1191.
31. Hale, M.E., Katz, H.R., Peek, M.Y., and Fremont, R.T. (2016). Neural circuits that drive startle behavior, with a focus on the Mauthner cells and spiral fiber neurons of fishes. *J. Neurogenet.* **30**, 89–100.
32. Mysore, S.P., and Kothari, N.B. (2020). Mechanisms of competitive selection: a canonical neural circuit framework. *eLife* **9**, e51473.
33. Yuille, A.L., and Grzywacz, N.M. (1989). A winner-take-all mechanism based on presynaptic inhibition feedback. *Neural Comput.* **1**, 334–347.
34. Maass, W. (2000). On the computational power of winner-take-all. *Neural Comput.* **12**, 2519–2535.
35. Fadok, J.P., Krabbe, S., Markovic, M., Courtin, J., Xu, C., Massi, L., Botta, P., Bylund, K., Müller, C., Kovacevic, A., et al. (2017). A competitive inhibitory circuit for selection of active and passive fear responses. *Nature* **542**, 96–100.
36. Shang, C., Chen, Z., Liu, A., Li, Y., Zhang, J., Qu, B., Yan, F., Zhang, Y., Liu, W., Liu, Z., et al. (2018). Divergent midbrain circuits orchestrate escape and freezing responses to looming stimuli in mice. *Nat. Commun.* **9**, 1232.
37. Hong, W., Kim, D.W., and Anderson, D.J. (2014). Antagonistic control of social versus repetitive self-grooming behaviors by separable amygdala neuronal subsets. *Cell* **158**, 1348–1361.
38. Koyama, M., Minale, F., Shum, J., Nishimura, N., Schaffer, C.B., and Fetcho, J.R. (2016). A circuit motif in the zebrafish hindbrain for a two alternative behavioral choice to turn left or right. *eLife* **5**, e16808.
39. Li, P., Geng, X., Jiang, H., Caccavano, A., Vicini, S., and Wu, J.Y. (2019). Measuring sharp waves and oscillatory population activity with the genetically encoded calcium indicator GCaMP6f. *Front. Cell. Neurosci.* **13**, 274.
40. Tovote, P., Fadok, J.P., and Lüthi, A. (2015). Neuronal circuits for fear and anxiety. *Nat. Rev. Neurosci.* **16**, 317–331.
41. Tovote, P., Esposito, M.S., Botta, P., Chaudun, F., Fadok, J.P., Markovic, M., Wolff, S.B.E., Ramakrishnan, C., Fenno, L., Deisseroth, K., et al. (2016). Midbrain circuits for defensive behaviour. *Nature* **534**, 206–212.
42. Muto, A., Ohkura, M., Kotani, T., Higashijima, S., Nakai, J., and Kawakami, K. (2011). Genetic visualization with an improved GCaMP calcium indicator reveals spatiotemporal activation of the spinal motor neurons in zebrafish. *Proc. Natl. Acad. Sci. USA* **108**, 5425–5430.
43. Akitake, C.M., Macurak, M., Halpern, M.E., and Goll, M.G. (2011). Transgenerational analysis of transcriptional silencing in zebrafish. *Dev. Biol.* **352**, 191–201.
44. Thisse, B., and Thisse, C. (2014). In situ hybridization on whole-mount zebrafish embryos and young larvae. *Methods Mol. Biol.* **1217**, 53–67.
45. Feldt, S., Waddell, J., Hetrick, V.L., Berke, J.D., and Zochowski, M. (2009). Functional clustering algorithm for the analysis of dynamic network data. *Phys. Rev. E Stat. Nonlin. Soft Matter Phys.* **79**, 056104.



## STAR★METHODS

### KEY RESOURCES TABLE

REAGENT or RESOURCE	SOURCE	IDENTIFIER
<b>Antibodies</b>		
rabbit anti-VACHT	Synaptic Systems	Cat# 139103 ; RRID: AB_887864
<b>Bacterial and virus strains</b>		
Subcloning Efficiency DH5 $\alpha$ Competent Cells	Life Technologies	Cat# 18265017
<b>Chemicals, peptides, and recombinant proteins</b>		
Tricaine	Sigma-Aldrich	Cat# A5040-25
Mecamylamine hydrochloride	Tocris Biosciences	Cat# 2843
(+)-D-tubocurarine chloride	Tocris Biosciences	Cat# 2820
Nicotine ditartrate	Acros Organics	Cat# N0590200
Tetrodotoxin	Tocris Biosciences	Cat# 1069
Baclofen	Tocris Biosciences	Cat# 0796
Cgp55845	Tocris Biosciences	Cat# 1248
Hoechst 33342	Life Technologies	Cat# H3570
Mowiol 4-88	Sigma-Aldrich	Cat# 475904
Pancurarium bromide	Sigma-Aldrich	Cat# P1918
NaCl	Sigma-Aldrich	Cat# S7653
KCl	Sigma-Aldrich	Cat# P9333
MgCl <sub>2</sub>	VWR/Avantor	Cat# 12315.A1
HEPES	Sigma-Aldrich	Cat# H4034
Glucose	Sigma-Aldrich	Cat# G6152
CaCl <sub>2</sub>	Sigma-Aldrich	Cat# C8106
Low melting agarose	Life Technologies	Cat# R0801
PFA	EMS	Cat# 15710
Glycerol	Sigma-Aldrich	Cat# G6279
T7 polymerase	NEB	Cat# M0251S
KpnI HF	NEB	Cat# R3142S
<b>Critical commercial assays</b>		
TOPO®TA cloning Kit	Life Technologies	Cat# 450640
Platinum Taq DNA Polymerase High Fidelity	Life Technologies	Cat# 11304011
<b>Experimental models: organisms/strains</b>		
<i>TgBAC(gng8:GAL4ff)<sup>c426</sup></i>	Hong et al. <sup>9</sup>	Zfin: ZDB-ALT-140423-2
<i>Tg(UAS:GCaMP7a)</i>	Muto et al. <sup>42</sup>	Zfin: ZDB-TGCONSTRCT-131030-2.
<i>Tg(UAS:GFP)<sup>c354</sup></i>	Akitake et al. <sup>43</sup>	ZDB-TGCONSTRCT-131029-7
<i>Tg(gad1b: R -GFP)</i>	Satou et al. <sup>20</sup>	ZDB-ALT-131127-6
<i>Tg(nptx2:Gal4-VP16)<sup>rw0143a</sup></i>	Agetsuma et al. <sup>5</sup>	ZDB-ALT-110215-5
<b>Oligonucleotides</b>		
Primer: gabbr1a Reverse	Cocco et al. <sup>19</sup>	N/A
Primer: gabbr1b Reverse	Cocco et al. <sup>19</sup>	N/A
Primer: gabbr1a Forward - ACGTATGGTTCCTCATCGGC	This paper	N/A
Primer: gabbr1b Forward - AGACAAGAGAAAGCACCTGGA	This paper	N/A

(Continued on next page)

**Continued**

REAGENT or RESOURCE	SOURCE	IDENTIFIER
<b>Software and algorithms</b>		
Fiji	Fiji	<a href="https://fiji.sc">https://fiji.sc</a> RRID:SCR_002285
MATLAB	Mathworks	<a href="https://www.mathworks.com/products/matlab/">https://www.mathworks.com/products/matlab/</a> RRID:SCR_001622
pClamp	Molecular Devices	<a href="https://www.moleculardevices.com/products/software/pclamp.html">https://www.moleculardevices.com/products/software/pclamp.html</a> RRID:SCR_011323
Clampfit 10	Molecular Devices	<a href="https://www.moleculardevices.com/products/software/pclamp.html">https://www.moleculardevices.com/products/software/pclamp.html</a>
HCIImage Live software	Hamamatsu, Japan	<a href="https://hcimage.com/">https://hcimage.com/</a>
ImageJ Mosaic Plug-ins	National Institute of Health, USA	<a href="https://ncmir.ucsd.edu/downloads/montaging_plugins.shtm">https://ncmir.ucsd.edu/downloads/montaging_plugins.shtm</a> RRID:SCR_001935
MetaMorph Microscopy Automation and Image Analysis Software	Molecular Devices	<a href="https://www.moleculardevices.com/Products/Software/Meta-Imaging-Series/MetaMorph.html">https://www.moleculardevices.com/Products/Software/Meta-Imaging-Series/MetaMorph.html</a> RRID:SCR_002368
GraphPad Prism	Molecular Devices	<a href="https://www.moleculardevices.com/products/software/pclamp.html">https://www.moleculardevices.com/products/software/pclamp.html</a>
R Project for Statistical Computing	R	<a href="http://www.r-project.org/">http://www.r-project.org/</a> RRID:SCR_001905
<b>Other</b>		
Perfusion peristaltic pump	Ismatec	<a href="http://www.ismatec.com/int_e/pumps/g_gearpumps/gearpumps.htm">http://www.ismatec.com/int_e/pumps/g_gearpumps/gearpumps.htm</a>
Spinning Disc Microscope - Axio Examiner.Z1	Zeiss	<a href="https://www.zeiss.com/microscopy/int/products/light-microscopes/axio-examiner-for-biology.html">https://www.zeiss.com/microscopy/int/products/light-microscopes/axio-examiner-for-biology.html</a>
SP5 laser scanning confocal microscope	Leica	<a href="https://www.leica-microsystems.com/fr/products/microscopes-confocaux/informations-detaillees/leica-tcs-sp5/">https://www.leica-microsystems.com/fr/products/microscopes-confocaux/informations-detaillees/leica-tcs-sp5/</a>
Epifluorescence Microscope BX51W1	Olympus	<a href="https://www.olympus-lifescience.com/en/microscopes/upright/bx61wi/">https://www.olympus-lifescience.com/en/microscopes/upright/bx61wi/</a>
Multiclamp 700B amplifier	Molecular Devices	<a href="https://www.moleculardevices.com/products/axon-patch-clamp-system/amplifiers/axon-instruments-patch-clamp-amplifiers">https://www.moleculardevices.com/products/axon-patch-clamp-system/amplifiers/axon-instruments-patch-clamp-amplifiers</a>
Digidata 1440 acquisition system	Molecular Devices	<a href="https://www.moleculardevices.com/sites/default/files/en/assets/user-guide/dd/cns/digidata-1440a-low-noise-data-acquisition-system.pdf">https://www.moleculardevices.com/sites/default/files/en/assets/user-guide/dd/cns/digidata-1440a-low-noise-data-acquisition-system.pdf</a>
Orca Flash4.0	Hamamatsu, Japan	<a href="https://www.hamamatsu.com/eu/en/product/type/C13440-20CU/index.html">https://www.hamamatsu.com/eu/en/product/type/C13440-20CU/index.html</a>
Orca 03G	Hamamatsu, Japan	<a href="http://www.hamamatsu.com.cn/UserFiles/DownFile/Product/20130929214608556.pdf">http://www.hamamatsu.com.cn/UserFiles/DownFile/Product/20130929214608556.pdf</a>
Vibratome VT1000 S	Leica	<a href="https://www.leicabiosystems.com/histology-equipment/sliding-and-vibrating-blade-microtomes/vibrating-blade-microtomes/leica-vt1000-s/">https://www.leicabiosystems.com/histology-equipment/sliding-and-vibrating-blade-microtomes/vibrating-blade-microtomes/leica-vt1000-s/</a>
Nikon Eclipse E800 microscope.	Nikon	<a href="https://www.microscopyu.com/museum/eclipse-e800">https://www.microscopyu.com/museum/eclipse-e800</a>

(Continued on next page)

### Continued

REAGENT or RESOURCE	SOURCE	IDENTIFIER
DS3 isolated constant current stimulator	Digitimer, Ltd.	<a href="https://www.digitimer.com/product/life-science-research/stimulators/ds3-isolated-current-stimulator/">https://www.digitimer.com/product/life-science-research/stimulators/ds3-isolated-current-stimulator/</a>
Master-8 pulse generator	A.M.PI	<a href="https://www.ampi.co.il/">https://www.ampi.co.il/</a>
Thermocycleur Doppio Gradient	VWR/Avantor	Cat# 732-2552

## RESOURCE AVAILABILITY

### Lead contact

Further information and requests for resources and reagents should be directed to and will be fulfilled by the Lead Contact, Elim Hong ([elim.hong@inserm.fr](mailto:elim.hong@inserm.fr)).

### Material availability

All plasmids generated in this study are available upon request to the Lead Contact.

### Data and code availability

- All data reported in this paper will be shared by the Lead Contact upon request.
- This paper does not report original code.
- Any additional information required to reanalyze the data reported in this paper is available from the Lead Contact upon request.

## EXPERIMENTAL MODEL AND SUBJECT DETAILS

AB wild-type and transgenic zebrafish lines *TgBAC(gng8:GAL4ff)<sup>c426</sup>*, *Tg(UAS:GCaMP7a)*, *Tg(nptx2:Gal4-VP16)<sup>rw0143a</sup>*, *Tg(gad1b:R|GFP)*, *Tg(UAS:GFP)<sup>c354 5,9,20,42,43</sup>* were used. Fish were maintained at 28°C on a 14:10h light: dark cycle in a recirculating system. All experiments were carried out in agreement with the European Directive 210/63/EU on the protection of animals used for scientific purposes and the French application decree 'Décret 2013-118'. The projects of our research group have been approved by the ethical committee 'Comité d'éthique Charles Darwin' (APAFIS#15909-2018070912072530 v5). The fish facility has been approved by the French 'Service for animal protection and health' (A-75-05-25).

## METHOD DETAILS

### Explant Dissection

*TgBAC(gng8:GAL4ff)<sup>c426</sup>;Tg(UAS:GCaMP7a)* 3, 6 and 7 day-post-fertilization (dpf) larvae were used for experiments. Larvae were anesthetized in Tricaine (0.01%) and brains dissected using fine forceps in ice cold Ringer's solution (134mM NaCl, 2.1 KCl, 1.2mM MgCl<sub>2</sub>, 10 mM HEPES, 10mM Glucose, 2.1 CaCl<sub>2</sub>, pH = 7.6) and mounted in 1.2% low melting agarose for calcium imaging and electrophysiology experiments.

### Pharmacology

Drugs were applied to the explants either directly using a pipette or by using a perfusion peristaltic pump (Ismatec) at a rate of 5-6 ml/min. Mecamylamine hydrochloride (100 μM), (+)-D-tubocurarine chloride (10 μM), nicotine ditartrate (10 μM, Acros Organics), tetrodotoxin (3 μM), baclofen (2 μM) and cgp55845 (1 μM) were used. The drugs were purchased from Tocris Bioscience unless otherwise noted.

### Calcium Imaging

Calcium imaging was performed on a spinning disk microscope (Zeiss Axio Examiner.Z1) using a 40X water immersion objective (NA = 0.95) or Leica SP5 laser scanning confocal microscope using a 25X water immersion objective (NA = 0.95). Images were acquired at a rate between 2.2-6.7Hz, depending on the experiment.

Nicotine was perfused for 5 minutes followed by E3 medium to wash out the drug. For experiments with mecamylamine hydrochloride and D-tubocurarine chloride, as a short-term application did not show any changes in calcium signals, we carried out the following experiment to assay for long-term change: baseline calcium signals were recorded for 15 minutes before pipetting the drug directly to the explant. The calcium signals were recorded for an additional 45 minutes after drug application. For the cgp55845 and baclofen experiments, 10-15 minutes baseline activity was recorded followed by drug application using the perfusion system and imaged for another 15 minutes.

### Patch-clamp recordings and simultaneous $\text{Ca}^{2+}$ imaging

Explants from *TgBAC(gng8:GAL4ff)<sup>c426</sup>;Tg(UAS:GCaMP7a)* larvae were placed in a recording chamber and constantly perfused with Ringer's solution at a rate of 1–2 mL/min. The IPN was made accessible for patch-clamp recordings and  $\text{Ca}^{2+}$  imaging by orienting the explants with the ventral surface upward. dHb terminals and the IPN were located and imaged using a 63x water immersion objective mounted on an epifluorescence microscope BX51W1 (Olympus) equipped with a 470 nm LED fluorescent excitation light. Patch electrodes were filled with an intracellular solution containing 130 mM CsMeSO<sub>4</sub>, 4 mM MgCl<sub>2</sub>, 4 mM Na-ATP, 0.3 mM Na-GTP, 10 mM HEPES, and 10 mM EGTA, 5 mM QX-314 adjusted to pH 7.2, 290 mOsm, for resistances between 5 and 8 M $\Omega$ . This intracellular solution allowed discrimination of cationic excitatory currents and chloride inhibitory currents based on their distinct reversal potentials ( $E_{\text{cation}} = 0$  mV;  $E_{\text{Cl}} = -60$  mV). By recording the cells at  $-60$  mV, EPSCs appeared as inward currents, whereas IPSCs were barely detectable. Conversely, IPSCs appeared as outward currents when recording the cells at a holding potential of  $-0$  mV, while EPSCs became undetectable. Whole-cell recordings were obtained using a Multiclamp 700B amplifier connected to a digitdata 1440 acquisition system monitored using pClamp 10 software (Molecular Devices). Analyses were performed using Clampfit 10 (Molecular Devices). For all experiments, data were filtered at 4 kHz during recording and the traces were digitized at 20 kHz.

Simultaneous time-lapse imaging of GCaMP fluorescence in dHb terminals was performed using either an Orca Flash4.0 (Hamamatsu, Japan) or Orca 03G (Hamamatsu, Japan) camera and recorded using the HC Image Live software (Hamamatsu, Japan) at an acquisition frequency of 5 Hz or 10 Hz with an exposure time of 200 ms and 100 ms, respectively. Time-lapse and patch-clamp acquisition were synchronized via a TTL signal sent to the camera via the pClamp 10 software. Time-lapse frames were encoded at a 256x256 pixel resolution using a 16-bit gray scale. Time-lapse images were analyzed using the ImageJ software (National Institute of Health, USA) and fluorescence signals were plotted using Clampfit 10.

### Immunohistochemistry

*TgBAC(gng8:GAL4ff)<sup>c426</sup>;Tg(UAS:GFP)<sup>c354</sup>* 6 dpf larvae were fixed in BT fix (4% PFA, 0.15mM CaCl<sub>2</sub>, 4% sucrose in 1x PBS) overnight in 4°C for rabbit anti-VACHT (1/200, Synaptic systems) labeling. Larvae were embedded in 4% low melt agarose and sectioned to 50  $\mu\text{m}$  using a vibratome (Leica, Inc). Floating sections were incubated in primary antibody in incubating solution (0.8% Triton-X in 1x PBS) for 3 days on a shaker in 4°C. The sections were washed and incubated in secondary anti-rabbit Alexa Fluor 594 (1:1000) with Hoechst 33342 (1:2000) overnight at 4°C on a shaker. *TgBAC(gng8:GAL4ff)<sup>c426</sup>;Tg(UAS:GFP)<sup>c354</sup>;Tg(gad1b:|R|GFP)* larvae were fixed overnight in 4% PFA, sectioned to 50  $\mu\text{m}$  and incubated with Hoechst 33342 (1:2000) overnight at 4°C on a shaker. All sections were then mounted on slides using Mowiol (Sigma). They were imaged using the Leica TCS SP5 AOBS upright microscope using a 63x (N.A. = 1.4) objective.

### RNA *in situ* Hybridization

PCR fragments for *gabbr1a* (ENSDARG00000018967) (553-bp) and *gabbr1b* (ENSDARG00000016667) (539-bp) were subcloned into pCRII-TOPO vector using the TOPO®TA cloning Kit (Invitrogen). Reverse primer sequences were from Cocco et al.<sup>19</sup> The following forward primers were used: *gabbr1a* (ACGTATGGTTCCTCATCGGC) *gabbr1b* (AGACAAGAGAAAGCACCTGGA). Restriction enzymes and RNA polymerase used to synthesize the antisense RNA probes are as follows: *gabbr1a* (KpnI/T7), *gabbr1b* (KpnI/T7). Colorimetric *in situ* hybridization (ISH) assay was performed as described in Thisse and Thisse<sup>44</sup> Following ISH, the larvae were mounted in 100% glycerol and imaged on a Nikon Eclipse E800 microscope.

### Electrical shock assay

Custom built electrical stimuli setup consisted of copper mesh electrodes that were mounted 6 cm apart on opposing sides and connected to a DS3 isolated constant current stimulator (Digitimer, Ltd.). Three electrical field stimulations (6mA, 20V, 500msec) were triggered every five minutes by MetaMorph (Molecular Devices). The larvae were paralyzed in 2% pancuronium bromide and mounted in the middle of 90mm diameter Petri dishes filled with 30 mL E3 medium to ensure consistent stimulation. Shock assay was performed in 6–7 dpf agarose-restricted larvae, paralyzed with 2% pancuronium bromide.

### Electrical stimulation

The IPN neurons were stimulated using a low-resistance (< 1M $\Omega$ ) glass pipette filled with Ringer solution containing an AgCl electrode. Train stimulations (20 $\mu\text{s}$  duration 50Hz stimulations lasting 400ms) were triggered every 1 minute with an isolated current stimulator (DS3; Digitimer Ltd.) using a Master-8 pulse generator (A.M.P.I.). Prior to each experiment, a dose-dependent curve was performed to select the optimal setting that induced negatively correlated events in the terminals at the IPN. Stimuli ranged between 100  $\mu\text{A}$  - 1.2 mA.

## QUANTIFICATION AND STATISTICAL ANALYSIS

### Calcium data analysis

Average fluorescence intensity of habenular soma was calculated by manually drawing regions of interest (ROI) in FIJI as described in Duboué et al.<sup>6</sup> To carry out a non-biased analysis of the dHb-IPN pathway and dHb terminals at the IPN, 2x2  $\mu\text{m}^2$  grid ROIs were drawn over the entire recording using FIJI macro. Average fluorescence intensity for each ROI was then extracted per frame and analyzed on MATLAB using custom written scripts.



Amplitude of calcium signal was calculated according to the formula:

$$\Delta F/F = (F_i - F_{\text{mean}})/F_{\text{mean}},$$

whereby,  $F_i$  is the mean intensity in a single ROI at a single time point while  $F_{\text{mean}}$  is the mean intensity in a single ROI throughout the entire recording time. Multiple clustering algorithms were tested including functional clustering algorithm<sup>45</sup> and spectral clustering on calcium traces and correlation coefficient values. After comparing the clusters generated using various algorithms, we found  $k$ -means and hierarchical clustering based on pairwise linear correlation matrix were the most representative of calcium signals in the spontaneous activity recordings.  $k$ -means and hierarchical clustering based on pairwise linear correlation matrix were carried out on MATLAB using *kmeans* and *linkage* functions ('euclidean' distance and 'complete' method), respectively. Different  $k$  values were tested and  $k = 5$  was selected based on manual inspection of calcium signals in the time-lapse recordings and also using a heatmap. The correlation matrix displayed in figures was generated by calculating the correlation coefficients between the average calcium signal traces for each cluster.

The threshold for hierarchical clustering was determined by manual inspection of the calcium signals in the recording and heatmap. Once specific IPN domains were identified by  $k$ -means, larger ROIs were manually drawn containing the different IPN domains. Analysis of calcium burst frequency using 'findpeaks' function was performed in MATLAB (Mathworks). Peak of calcium burst, calcium inhibition and half duration were identified using *findpeaks* and *half prominence* functions in MATLAB and verified manually. Calcium burst peak was defined by the highest value during a calcium burst. Peak of calcium inhibition was defined by the lowest value during a calcium inhibition event. Half duration was calculated as the width of the calcium signal at the half value of a peak during a calcium burst or inhibition. All graphs and plots were made on MATLAB using custom written scripts.

### Statistical analysis

Statistical tests were carried out using a Wilcoxon signed rank test for averaged paired samples, Kruskal-Wallis test followed by a Dunn's test for comparison between more than 2 groups, Mann-Whitney test was used with independent samples and a linear mixed model with fixed effect was used to compare multiple values from repeated events. All statistical tests were performed on R or GraphPad Prism (GraphPad Software, Inc.).  $p < 0.05$  was considered as statistically significant. All statistical details including statistical tests, exact values of  $n$ , value representation (mean  $\pm$  SD) are indicated in the figure legends.